PASJ: Publ. Astron. Soc. Japan , –?? (2008)

arXiv:astro-ph/0004220v1 17 Apr 2000

J-Net Galactic Plane Survey of VLBI Radio Sources for VLBI Exploration of Radio Astrometry (VERA)

Mareki Honma[1,2], Tomoaki Oyama[1,3], Kazuya Hachisuka[1,5], Satoko Sawada-Satoh[1,2], Kouichi Sebata[1,9], Makoto Miyoshi[1,4], Osamu Kameya[1,2], Seiji Manabe[1,2,4], Noriyuki Kawaguchi[1,4], Tetsuo Sasao[1,4], Seiji Kameno[6], Kenta Fujisawa[6], Katsunori M. Shibata[4,6], Takeshi Bushimata[6], Takeshi Miyaji[1,7], Hideyuki Kobayashi[6], Makoto Inoue[6,7], Hiroshi Imai[1,2,4], Hiroshi Araki[2], Hideo Hanada[4], Kenzaburo Iwadate[2], Yoshihisa Kaneko[4], Seisuke Kuji[4], Katsuhisa Sato[2], Seiitsu Tsuruta[2], Satoshi Sakai[4], Yoshiaki Tamura[4], Koji Horiai[2], Tadayoshi Hara[4], Koichi Yokoyama[4], Junichi Nakajima[8], Eiji Kawai[8], Hiroshi Okubo[8], Hiro Osaki[8], Yasuhiro Koyama[8], Mamoru Sekido[8], Tomonari Suzuyama[8], Ryuichi Ichikawa[8], Tetsuro Kondo[8], Kensei Sakai[10], Katsuhiro Wada[10], Naohiko Harada[10], Norihiro Tougou[10], Mitsumi Fujishita[10], Rie Shimizu[11], Satomi Kawaguchi[11], Akane Yoshimura[11], Masakazu Nakamura[11], Wataru Hasegawa[11], Satoshi Morisaki[11], Ryuichi Kamohara[11], Tomoe Funaki[11], Naoko Yamashita[11], Teruhiko Watanabe[11], Tomomi Shimoikura[11], Masanori Nishio[11], Toshihiro Omodaka[11], Atuya Okudaira[12]

[1] *VERA Project Office, NAOJ, Mitaka, Tokyo, 181-8588*
[2] *Mizusawa Astrogeodynamics Observatory, NAOJ, Mizusawa, Iwate 023-0861*
[3] *Department of Astronomy, University of Tokyo, Bunkyou, Tokyo 113-8654*
[4] *Earth Rotation Division, NAOJ, Hoshigaoka, Mizusawa, Iawate 023-0861*
[5] *Graduate University for Advanced Studies, Hayama, Kanagawa 240-01*
[6] *VSOP Project, NAOJ, Mitaka, Tokyo, 181-8588*
[7] *Nobeyama Radio Observatory, NAOJ, Minamisaku, Nagano 384-1305*
[8] *Kashima Space Research Center, Communications Research Laboratory, Kashima, Ibaraki 314-0012*
[9] *Communications Research Laboratory, Koganaei, Tokyo 184-8795*
[10] *School of Engineering, Kyushu-Tokai Univerisity, Kumamoto 862-8652*
[11] *Faculty of Science, Kagoshima University, Kagoshima 890-0065*
[12] *International University of Kagoshima, Kagoshima 891-0191*
E-mail(MH): honmamr@cc.nao.ac.jp

(Received ; accepted)

Abstract

In order to search for new VLBI sources in the Galactic plane that can be used as phase reference sources in differential VLBI, we have conducted 22 GHz observations of radio sources in the Galactic plane using the Japanese VLBI Network (J-Net). We have observed 267 VLBI source candidates selected from existing radio surveys and have detected 93 sources at the signal-to-noise ratio larger than 5. While 42 of the 93 detected sources had already been detected with VLBI at relatively lower frequency (typically 2 to 8 GHz), the remaining 51 are found to be new VLBI sources detected for the first time. These VLBI sources are located within $|b| \leq 5^\circ$, and have a large number of Galactic maser sources around them. Thus, they are potential candidates for phase reference sources for VLBI Exploration of Radio Astrometry (VERA), which is the first VLBI array dedicated to the phase referencing VLBI astrometry aiming at measuring the parallax and proper motion of maser sources in the whole Galaxy.

Key words: radio sources — radio galaxies — QSOs — VERA

1. Introduction

VLBI Exploration of Radio Astrometry (VERA), approved to start its construction in 2000, is a new Japanese VLBI array of 20m antennas dedicated to astrometry (Honma et al. 2000; Kawaguchi et al. 2000). VERA will undertake astrometry of Galactic maser sources based on the differential VLBI technique, in which two adjacent sources are observed simultaneously to remove the atmospheric fluctuation. A position accuracy of ~ 100 μarcsec has been already achieved by switching differential VLBI in which an object and a reference are observed by turns (e.g., Lestrade et al. 1999), but the atmospheric fluctuation is not completely suppressed because of the time lag between observations of an object and a reference. In order to obtain a higher position accuracy, one needs to observe an object and a reference source at the same time. VERA, with its dual beam antenna system, will enable us to observe a Galactic maser and an extragalactic reference source simultaneously. With such a system, positions of maser sources relative to reference sources can be measured with 10 μarcsec level accuracy, allowing us to obtain parallaxes of maser sources in the whole Galaxy.

To remove the atmospheric fluctuation effectively, a reference source must be sufficiently close to the maser source for which one intends to measure the parallax and proper motion. In order for VERA to achieve a 10 μarcsec level accuracy, it is required that a maser and a reference source must be located within 2° from each other. This requires a large number of reference sources spreading over the whole sky area. Currently, there exist several catalogs that contain hundreds of continuum sources detected with VLBI (e.g., Preston et al. 1985; Morabito et al. 1986; Johnston et al. 1995; Ma et al. 1998; Peck & Beasley 1998). In total, more than 2000 VLBI sources are known. However, the number of VLBI sources is considerably smaller in the Galactic plane than that in the off-plane region. This is because several surveys of VLBI sources were conducted in the off-plane regions: for example, the VLBI survey by Preston et al.(1985) are for $|b| \geq 10°$, and the VLBA calibrator survey by Peck & Beasley (1998) are mainly based on the Jodrell Bank-VLA Astrometric Survey (Patnaik et al. 1992; Browne et al. 1998; Wilkinson et al. 1998), which are conducted at $|b| \geq 2.5°$. On the other hand, H_2O and SiO masers, which are the main targets of VERA, are mostly concentrated in the Galactic plane because they are emitted from Galactic star forming regions and Mira-type variable stars: for example, about 40% of H_2O maser sources listed in Palagi et al.(1993) are located within $b = \pm 5°$. Therefore, a large number of VLBI sources are necessary as phase and position reference for VERA, and hence the search for VLBI sources in the Galactic plane is indispensable to the success of VERA.

A search for VLBI sources in the Galactic plane has its own scientific merits even apart from the necessity for VERA. First, many of the continuum radio sources are likely to be radio galaxies and QSOs, and so a search for radio sources in the Galactic plane will provide a basis for studying the distribution of galaxies and large scale structures behind the Milky Way. Second, a search for VLBI sources in the Galactic plane may lead us to discoveries of new active Galactic sources like X-ray binaries or flare stars which are of significant interest in stellar physics and high energy astrophysics. Third, the radio sources can be used to study the cold interstellar matter in the Galaxy by observing the absorption line systems toward them, and also can be used to investigate the ionized interstellar matter by evaluating the interstellar scintillation effect on these sources. Hence, a search for radio sources in the Galactic plane is useful not only for VERA, but also for a number of interesting studies in astronomy and astrophysics. For these reasons, we have performed a survey of continuum radio sources in the Galactic plane using the Japanese VLBI Network (hereafter J-Net; Kameya et al. 1993; Shibata et al. 1994; Omodaka et al. 1994) at 22GHz, and here we report on the results.

2. Sample Selection

In order to find VLBI sources effectively, we selected VLBI source candidates from existing radio surveys. The source candidates in the northern sky ($\delta \geq 0°$) were selected from the single-dish sky survey made at Green Bank (Becker et al. 1991, hereafter Green Bank survey) and the low resolution interferometer survey made with the Texas interferometer (Douglas et al. 1996, hereafter Texas survey). The northern VLBI source candidates were selected under the following selection criteria: 1) sources that are listed both in Green Bank survey and Texas survey, 2) sources that are located at $|b| \leq 5°$, 3) sources that have an expected flux density at 22 GHz larger than 100 mJy (calculated from flux density at 5 GHz in Green Bank survey and at 0.3GHz in Texas survey), and 4) sources that are not classified as an extended source in the Green Bank survey. The last condition was introduced because highly extended sources are likely to be resolved out when observed with VLBI. The number of VLBI source candidates selected under these criteria is 198.

To examine whether the sources selected under such criteria are likely to be VLBI sources, we applied the criteria 1), 3) and 4) to the radio sources located at $b \geq 30°$, where a large number of VLBI sources are listed in the International Celestial Reference Frame catalog (Ma et al. 1998, hereafter ICRF catalog) and VLBA calibrator survey (Peck & Beasley 1998). We confirmed that more than 40% of sources which are at $b \geq 30°$ and satisfy the criteria 1), 3) and 4) are indeed known VLBI sources listed in ICRF catalog or VLBA calibrator survey.

Since part of the southern sky is also observable with J-Net and VERA, VLBI source candidates were also selected in the southern Galactic plane. Similar to the northern sample, the southern sample sources were selected based on the following criteria: 1) sources that are listed both in Parkes-MIT-NRAO survey (Griffith et al. 1994; 1995, hereafter PMN survey) and Texas survey, 2) sources that are located in the southern Galactic plane observable with J-Net ($|b| \leq 5°$, $0° \leq l \leq 33°$ or

$213° \leq l \leq 243°$), 3) sources that have a flux larger than 200 mJy at 5 GHz, and 4) sources that are not classified as an extended source in the PMN survey. The total number of the sources which satisfy the criteria above are 86. Including 198 northern VLBI source candidates, our sample consists of 284 continuum sources located at $0° \leq l \leq 243°$ and $-5° \leq b \leq 5°$. Table 1 lists the 284 VLBI source candidates with positions taken from Texas survey. As discussed later, some of the sources in table 1 are already known as VLBI sources. Nevertheless, they were included in the source list and observed with J-Net because measurements of their correlated flux density at 22 GHz are necessary for VERA. For known VLBI sources, we present in table 1 the most accurate positions taken from ICRF catalog and VLBA calibrator survey.

3. Observation and Data Reduction

The observation was carried out at 22 GHz during Oct 7 - 11, 1999 (100 hours in total) using J-Net, which consists of four stations; Nobeyama 45m, Kashima 34m, Mizusawa 10m and Kagoshima 6m. Since the main purpose of this observation is to detect as many sources as possible, integration time was set to be quite short, typically 5 minutes. This integration time is longer than a typical VLBI coherence time at 22 GHz ($\sim$ 100 sec), and thus sufficient for fringe search. In order not to miss some detections due to bad weather or system trouble, most of sources were observed twice or more. Strong H_2O maser sources, which were used to check the system performance and to calibrate the flux of continuum sources, were also observed approximately every two hours with an integration time of 5 minutes. Known VLBI sources were also observed frequently to calibrate clock offsets in the hydrogen-maser frequency standard at each station. Signals were sampled at the rate of 32×10^6 sample per second with 2-bit quantization, and recorded at the rate of 128 Mbps using the VSOP terminal with two baseband channels of 16 MHz bandwidth. In order to avoid detecting H_2O masers at the band edge, the frequency coverage of the two channels were set to overlap slightly, covering from 22.220 GHz to 22.250 GHz in total. The correlation processing was carried out with the Mitaka FX correlator (Chikada et al. 1991) located at NAOJ Mitaka campus, and fringe search was made using Global Fringe Search (GFS) procedure. The size of the fringe search window was 1 μsec by 20 psec/sec in residual delay and delay rate, respectively. Fringe search was mainly done for the Nobeyama-Kashima baseline, which has the shortest baseline and highest sensitivity among six J-Net baselines, and other baselines were used supplementary, in particular for position measurements (see section 4.3).

4. Results

4.1. Fringe Detection

Out of 284 sources listed in table 1, we observed 267 sources, including 51 previously-known VLBI sources that are listed in any of ICRF catalog (Ma et al. 1998), VLBA calibrator survey (Peck & Beasley 1998) or 2 GHz VLBI survey (Preston et al. 1985; Morabito et al. 1986). Out of 267 observed sources, 93 sources were detected with Nobeyama-Kashima baseline at the signal-to-noise ratio (S/N) larger than 5. This detection criterion corresponds to a confidence level of 99.5%. The S/N for Nobeyama-Kashima baseline is listed in table 1. The total detection rate of the sources listed in table 1 is about 35 % (=93/267). This relatively high detection rate suggests that the simple selection criteria described in section 2 work quite effectively as selection criteria for VLBI sources. Hence, such selection criteria may be useful for further searches for VERA's reference sources at any Galactic latitude. We note that the detection limit of VERA array is not so different from that of J-Net Nobeyama-Kashima baseline. While the product of aperture diameter for Nobeyama-Kashima baseline is about four times larger than that of a VERA baseline, the recording rate of VERA array will be 1G bit per second, which is eight times higher than that of J-Net. Thus, the detection limit of Nobeyama-Kashima baseline is lower than that of a VERA baseline by only a factor of 1.35.

Among 93 sources detected in the present study, 42 were known VLBI sources. Since the number of observed known VLBI sources was 51, the 22 GHz detection rate of known VLBI sources is 82%. Note that these known VLBI sources were mostly discovered at relatively low frequency (typically from 2 to 8 GHz) and selected based on the flux estimates described in section 2. The high detection rate in the present study indicates that our flux estimates based on the low resolution observations worked relatively well.

As for the remaining 51 detected sources, detections were not reported in any literature. Thus, as far as we know, these 51 sources were detected with VLBI for the first time. Figure 1 shows the distribution of the new VLBI sources in Galactic coordinates as well as other sources listed in table 1. From figure 1 one can see that the newly detected VLBI sources are distributed almost randomly in the Galactic plane within $|b| \leq 5°$ and $0° \leq l \leq 243°$. However, the detection rate at the Galactic center region is smaller than that in the other regions. Possible reasons for this are: 1) maximum elevations of the sources at the Galactic center region are quite low, and thus relatively high system noise temperature makes it difficult to detect them; 2) the high column density of interstellar plasma toward the Galactic center region causes strong interstellar scintillation and thus the radio sources are resolved out when observed with

VLBI; and/or 3) since star formation activity is significantly higher near the Galactic center, many of the VLBI source candidates at the Galactic center region may be compact HII regions that are resolved out with VLBI.

4.2. Flux Measurement

For 93 detected sources, we obtained the correlated flux density for the Nobeyama-Kashima baseline. The correlated flux density was calculated using the following relation,

$$S = \frac{2k\rho}{\eta_c} \frac{\sqrt{T_{\rm sys1} T_{\rm sys2}}}{\sqrt{\eta_{e1}\eta_{e2} A_1 A_2}}. \qquad (1)$$

Here ρ is the correlation coefficient, $T_{\rm sys}$ is the system noise temperature, A is the antenna aperture, η_e is the antenna efficiency, k is the Boltzmann constant, and η_c is the sampling efficiency which equals to 0.88 for the 2-bit sampling mode. The antenna aperture of Nobeyama and Kashima stations are 1590 $\rm m^2$ (45mϕ) and 908 $\rm m^2$ (34mϕ), and the aperture efficiencies are 0.60 and 0.57, respectively. The correlation coefficient ρ was calculated with GFS procedure by integrating the observational data within the coherence loss limit. Typical timescale of the coherence loss was found to be ~120 seconds. The system noise temperature $T_{\rm sys}$ was monitored roughly every two hours at both Kashima and Nobeyama stations based on the R-Sky method, in which a blank sky and a reference black body were observed. To correct for the elevation differences for each source, we converted $T_{\rm sys}$ into the optical depth at the zenith τ_0, which relates to $T_{\rm sys}$ through the following equation,

$$T_{\rm sys} \exp(-\tau_0 \sec z) = T_{\rm RX} + T_{\rm atm} \left(1 - \exp(-\tau_0 \sec z)\right). \qquad (2)$$

Here $T_{\rm RX}$ is the receiver noise temperature, $T_{\rm atm}$ is the atmospheric temperature, and z is the zenith distance. Note that a factor of $\exp(-\tau_0 \sec z)$ in the left-hand side corrects for the atmospheric attenuation. The atmospheric temperature $T_{\rm atm}$ at both stations is assumed to be 290K, which is accurate within 3% during the observation. The receiver temperature at the Kashima station was 240K with its variation of ~ 3% during the observation period. The receiver temperature at Nobeyama station was estimated to be 100K from the $T_{\rm sys}$ dependence on the $\sec z$, and assumed to be constant during the observation.

The correlated flux densities for 93 sources were calculated from equation (1) and are listed in table 1. Since all detected sources have S/N ratio larger than 5, the error in flux density caused by the correlation coefficient measurement is less than 20%. However, the variation of atmospheric condition with timescale shorter than two hours (the timescale of $T_{\rm sys}$ measurement) is another cause for errors in flux density measurement, and thus the typical error of flux density in table 1 is not much less than ~ 20%. Figure 2 shows the number distribution of correlated flux densities. As seen in figure 2, the number of sources increases in a power law form with decreasing the flux density, as usually expected. Figure 2 also demonstrates that while bright sources were mostly detected with previous observations, many of faint sources are detected for the first time by our observation.

4.3. Position measurement

Some of the sources we observed were detected with multiple baselines. For the sources which are detected with 3 or more independent baselines, we estimated the source position using the delay rate. The delay rate and the source position are related to each other through following equation:

$$c\Delta\dot{\tau}_g = \dot{U}\Delta x + \dot{V}\Delta y, \qquad (3)$$

where c is the speed of light, U and V are physical baseline length projected onto the u-v plane, and the dot indicates the time derivative. The observable $\Delta\dot{\tau}_g$ is defined as the difference between the observed geometric delay rate and the predicted geometric delay rate calculated from the given source positions and baseline parameters. This difference in the delay rate is caused by the position offset Δx and Δy, which is defined as the difference between the position of phase tracking center (position given in table 1) and the real source. Note that Δx is measured in the direction of right ascension and Δy is measured in the direction of declination, as commonly done. The geometric delay rate difference $\Delta\dot{\tau}_g$ as well as the time derivative of baseline components U and V were calculated with GFS procedure.

In table 2, we list the positions for 21 sources that are detected with 3 or more baselines. Note that all of 21 sources are new VLBI sources except TXS0601+245, which was detected by Morabito et al.(1986), but accurate position was not reported. Because of short observation (typically 5 minutes for each source) and relatively short baselines (for example, Nobeyama-Kashima baseline is 197 km, and Nobeyama-Mizusawa baseline is 425 km), the positional accuracy is of ~ 1 arcsec. As seen in table 2, the positions obtained with Texas survey (listed in table 1) are usually accurate within a few arc-seconds, but there are some sources showing position errors larger than 10 arc-seconds. Thus, one has to be careful in search for an optical counterpart of Texas sources.

5. Discussion

As seen in previous sections, we have detected 93 of 267 Texas survey sources that are selected under simple criteria, and found 51 new VLBI sources in the Galactic plane. The total detection rate of 35%(=93/267) is quite high, and thus one can use the same criteria to search for more VLBI sources in the other sky area. Also, the 22 GHz detection rate of known VLBI sources that were previously detected at relatively low frequency (typically 2 to 8 GHz) are quite close to unity.

Since the detection limit of J-Net is quite close to that of VERA, most of the sources detected in the present study are also observable with VERA. Thus, one can expect that the discovery of 51 new VLBI sources increases significantly the number of maser-QSO pairs that can be observed with VERA. In fact, there are 129 H_2O maser sources within 2° of 51 new VLBI sources, according to the H_2O maser catalog by Palagi et al.(1993). This number roughly corresponds to 1/6 of independent H_2O maser sources in Palagi et al.(1993). Thus, the sources detected in this study will be of great use as reference sources for VERA.

In order to use the radio sources discovered in the present study (and also other sources) as reference for differential VLBI, one has to know the nature of sources, particularly whether the source is a Galactic or extra-Galactic object. If the source is a Galactic object, then its parallax and proper motion are not negligible, being unsuitable for position reference. The best way to know the source nature is optical-identification and spectroscopic measurement of source redshifts. Unfortunately, optical counterparts and their redshifts are known for only few sources in table 1. This is partly because positions obtained with single dish and low resolution interferometer observations are not accurate enough for optical identification, and partly because the sources in the Galactic plane suffer significantly from Galactic extinction at the optical band.

The problem of position accuracy can be resolved by measuring its position with VLBI at an accuracy of 1 arcsec or less. As described in section 4, accurate portions of 21 sources that were detected with 3 or more baselines are obtained in the present study. In the Digital Sky Survey images, we have found 7 possible optical counterparts, but redshifts are given for only 1 of them in the NASA Extra-galactic Database. Thus, spectroscopic observation of these optical counterparts are required to understand the source nature.

The fact that possible optical counterparts are found for about 1/3 of the sources with accurate positions is encouraging for further study of the nature of these radio sources in the Galactic plane. If deep observations are carried out at optical or infrared wavelengths, one may be able to find optical counterparts for a large number of VLBI sources in the Galactic plane, provided that accurate positions are available. Therefore, the next step to understand their nature is to measure source positions at 1 arcsec level, and this can be easily achieved using current VLBI technique.

6. Conclusion

We have searched for new VLBI sources in the Galactic plane using J-Net. We have observed 267 sources that are selected from single dish and low resolution interferometer observations, and detected 93 sources including 51 sources that are detected with VLBI for the first time. We have presented the correlated flux for Nobeyama-Kashima baseline for all sources we detected, and also positions for 21 sources that are detected with 3 or more baselines. These VLBI sources are located within $|b| \leq 5°$ of the Galactic plane, and there are a large number of maser sources within 2° of them. Thus, the sources detected in the present study are potential candidates for the reference sources of phase-referencing VLBI astrometry with VERA.

acknowledgment

We are grateful to the NRO staffs, especially Drs. N.Ukita, K.Sunada and N.Nakai, for kindly providing us the observation time of the 45m telescope as a part of their supports to the VERA project. We also thank the referee for careful reading the manuscript and several constructive suggestions. Parts of data reduction in the present study were carried out on the workstations at Astronomical Data Analysis Center of the National Astronomical Observatory, Japan.

figure caption

Figure 1 : Distribution of observed radio sources in Galactic coordinates. Filled circles are 51 new VLBI sources, and open circles are 42 previously known VLBI sources that are also detected at 22 GHz in the present study. Crosses are the radio sources that were observed but not detected.

Figure 2 : Distribution of correlated flux density at 22 GHz for Nobeyama-Kashima baseline. Filled area shows distribution of correlated flux density for previously known VLBI sources.

References

Becker R.H., White R.L., Edwards A.L. 1991, ApJS 75, 1

Browne I.W.A., Patnaik A.R., Wilkinson P.N., Wrobel J.M. 1998, MNRAS 293, 257

Chikada et al. 1991, in *Frontiers of VLBI*, eds. Hirabayashi et al., Universal Academy Press (Tokyo), p79

Douglas J.N., Bash F.N., Bozyan F.A., Torrence G.W., Wolfe C. 1996, AJ 111, 1945

Johnston K.J., Fey A.L., Zacharias N., Russell J.L., Ma C., de Vegt C., Reynolds J.E., Jauncey D.L., Archinal B.A., Carter M.S., Corbin T.E., Eubanks T.M., Florkowski D.R., Hall D.M., McCarthy D.D., McCulloch P.M., King E.A., Nicolson G., Shaffer D.B. 1995, AJ 110, 880

Griffith M.R., Wright A.E., Burke B.F., Ekers R.D. 1994, ApJS 90, 179

Griffith M.R., Wright A.E., Burke B.F., Ekers R.D. 1995, ApJS 97, 347

Honma M., Kawaguchi N., Sasao T. 2000, in Proc. of SPIE Vol.4015 *Radio Telescope*, eds H. R. Buthcer, in press

Kameya O., Sasao T., Kawano N., Hara T., Kuji S., Iwadate K., Tsuruta S., Asari K., Tamura Y., Yasuda S., Morimoto M., Miyazawa K., Kawaguchi N., Miyaji T. 1993, in Proc. of the Second North-Asian Regional Meeting *Recent Developement in Millimeter-Wave and Infrared Astronomy*, eds S.H. Cho and H.S. Chung, Terra Scientific Publishing Company (Tokyo) pp16-20

Kawaguchi N., Sasao T., Manabe S. 2000, in Proc. of SPIE Vol.4015 *Radio Telescope*, eds H. R. Buthcer, in press

Lestrade J.F., Preston R.A., Jones D.L., Phillips R.B., Rogers A.E.E., Titus M.A., Rioja M.J., Gabuzda D.C. 1999, A&A 344, 1014

Ma C., Arias E.F., Eubanks T.M., Fey A.L., Gontier A.M., Jacobs C.S., Sovers O.J., Archinal B.A., Charlot P. 1998, AJ 116, 516

Morabito D.D., Niell A.E., Preston R.A., Linfield R.P., Wehrle A.E., Faulkner J. 1986, AJ 91, 1038

Omodaka T., Morimoto M., Kawaguchi N., Miyaji T., Yasuda S., Suzuyama T., Kitagawa T., Miyazaki T., Furuya L., Jike T., Miyazawa K., Mikoshiba H., Kuji S., Kameya O. 1994, in *VLBI TECHNOLOGY - Progress and Future Observational Possibilities*, eds Sasao T., Manabe S., Kameya O., Inoue M., Terra Scientific Publishing Company (Tokyo), pp191-195

Palagi F., Cesaroni R.,Comoretto G., Felli M., Natale V. 1993, A&AS 101, 153

Patnaik A.R., Browne I.W.A., Wilkinson P.N., Wrobel J.M., 1992, MNRAS 154, 655

Peck A.B., Beasley A.J. 1998, in *Radio Emission from Galactic and Extragalactic Compact Sources*, ASP Conference Series Vol.144, IAU Colloquium 464, eds, J.A. Zensus, G.B. Taylor, and J.M. Wrobel, p.155

Preston R.A., Morabito D.D., Williams J.G., Faulkner J., Jauncey J., Nicolson G.D. 1985, AJ 90, 1599

Shibata K.M., Asaki Y., Asari I., Fukuzaki Y., Hara T., Horiai K., Iwadate K., Kameya O., Kawano N., Kuji S., Manabe S., Sakai S., Sasao T., Sato K., Tamura Y., Tsuruta S. 1994, in *VLBI TECHNOLOGY - Progress and Future Observational Possibilities*, eds Sasao T., Manabe S., Kameya O., Inoue M., Terra Scientific Publishing Company (Tokyo), pp185-190

Wilkinson P.N., Browne I.W.A., Patnaik A.R., Wrobel J.M.,Sorathia B. 1998, MNRAS 300, 790

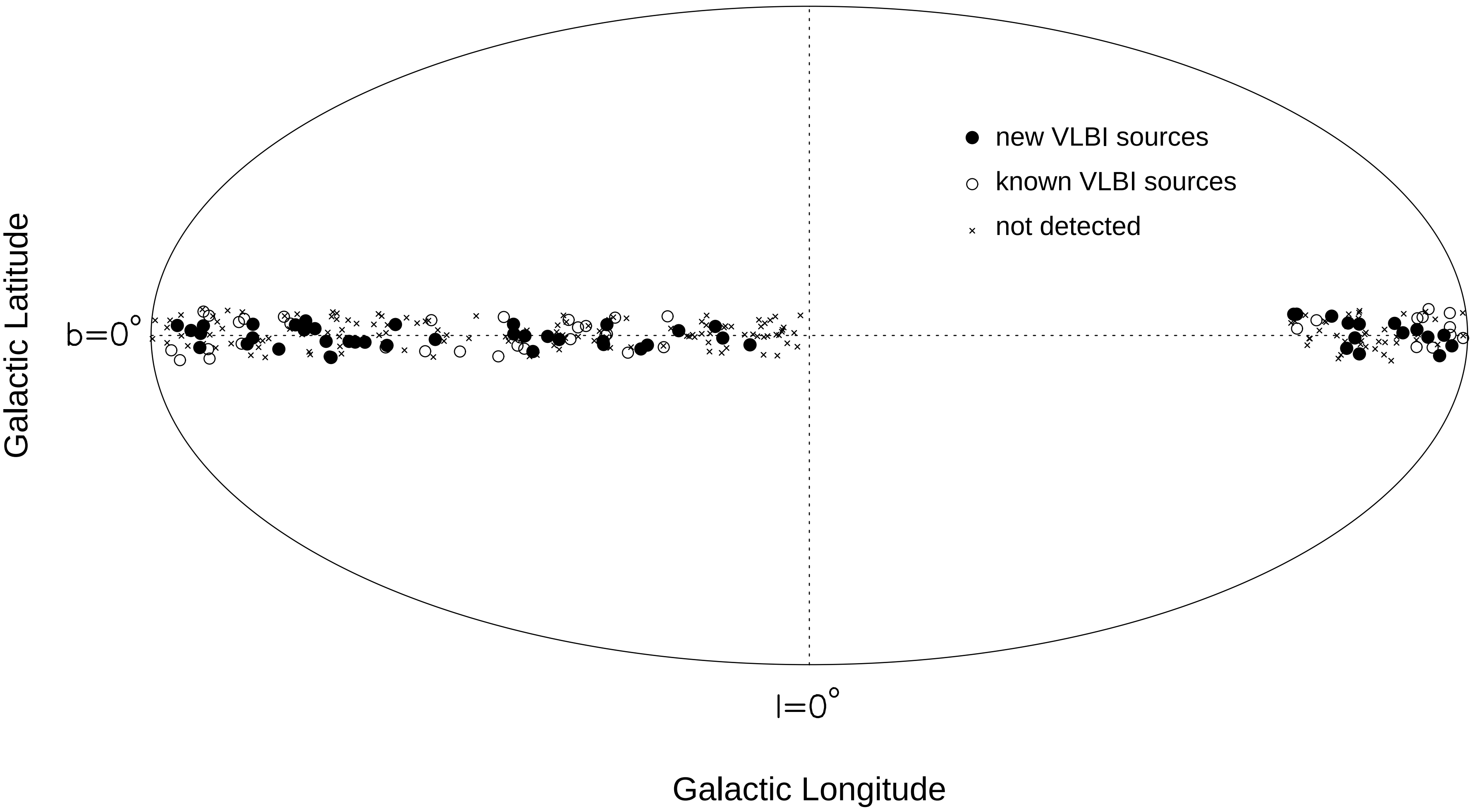
● new VLBI sources
○ known VLBI sources
× not detected
b=0°
l=0°
Galactic Latitude
Galactic Longitude

arXiv:astro-ph/0004220v1 17 Apr 2000

Table 1. List of 284 VLBI source candidates.

Name	RA(J2000)	Dec(J2000)	l (°)	b (°)	S/N	$S_{22\mathrm{G}}$	Note
TXS2358+605	00 01 07.4	+60 51 25	116.84	-1.42	7.5	109	
TXS0009+655	00 12 37.6	+65 51 11	118.97	3.28	...	...	
TXS0012+610	00 14 48.7	+61 17 45	118.55	-1.26	13.5	206	
TXS0026+637	00 29 44.8	+63 58 43	120.56	1.21	...	...	
TXS0033+586	00 36 07.7	+58 55 47	120.95	-3.88	...	...	
TXS0034+623	00 37 04.6	+62 36 30	121.28	-0.22	...	...	
TXS0034+602	00 37 24.2	+60 29 51	121.20	-2.33	...	...	
TXS0041+660	00 44 41.3	+66 18 42	122.25	3.45	...	...	
TXS0042+672	00 45 42.1	+67 33 21	122.38	4.69	...	...	
TXS0055+675	00 58 19.4	+67 49 01	123.58	4.95	...	...	
TXS0056+579	00 59 52.2	+58 12 24	124.05	-4.65	15.5	231	
TXS0056+665	01 00 03.8	+66 50 58	123.78	3.99	...	...	
TXS0059+581	01 02 45.7630	+58 24 11.139	124.42	-4.44	26.0	444	IV
TXS0103+631	01 06 29.7	+63 26 06	124.61	0.61	...	...	
TXS0106+612	01 09 46.6	+61 33 31	125.11	-1.24	16.7	219	
TXS0137+635	01 40 43.1	+63 46 07	128.35	1.42	12.4	165	
TXS0141+579	01 45 14.2993	+58 10 49.783	129.99	-3.95	...	...	V
TXS0144+584	01 47 46.5438	+58 40 44.975	130.21	-3.39	...	...	V
TXS0203+625	02 07 02.7	+62 46 13	131.46	1.16	17.4	226	
TXS0205+643	02 09 36.0	+64 37 26	131.18	3.01	14.1	169	
TXS0205+614	02 09 37.9	+61 40 55	132.06	0.20	...	...	
TXS0219+628	02 23 29.2	+63 07 17	133.12	2.08	...	...	
TXS0227+626	02 31 59.0	+62 50 36	134.12	2.18	5.6	71	
TXS0233+647	02 37 50.4	+64 57 55	133.89	4.38	...	...	
TXS0237+612	02 41 33.8	+61 26 29	135.70	1.33	...	...	
TXS0241+622	02 44 57.6968	+62 28 06.514	135.64	2.43	47.8	799	I
TXS0248+560	02 51 54.8	+56 16 20	139.13	-2.76	35.2	495	
TXS0301+627	03 05 53.9	+62 57 22	137.55	3.96	...	...	
TXS0302+625	03 06 42.6611	+62 43 02.022	137.75	3.80	8.9	118	IV
TXS0309+525	03 12 50.7	+52 45 25	143.49	-4.38	...	...	
TXS0314+565	03 17 55.1	+56 43 42	142.03	-0.61	...	...	
TXS0323+551	03 27 18.6	+55 20 28	143.89	-1.06	...	...	
TXS0326+533	03 29 52.2	+53 32 34	145.21	-2.33	...	...	
TXS0331+544	03 34 56.0	+54 37 23	145.20	-1.02	...	...	
TXS0334+506	03 37 43.3	+50 45 53	147.81	-3.90	...	...	
TXS0342+538	03 46 32.0	+54 01 25	146.91	-0.49	13.2	177	
TXS0346+514	03 50 24.9	+51 38 37	148.85	-1.99	...	...	
TXS0346+518	03 50 44.4	+52 01 22	148.65	-1.66	5.1	49	
TXS0354+559	03 58 30.0	+56 06 44	146.92	2.21	30.8	436	
TXS0355+508	03 59 29.7477	+50 57 50.161	150.38	-1.60	330.3	3864	IV
TXS0410+486	04 14 39.2	+48 48 14	153.64	-1.57	...	...	
TXS0414+548	04 18 19.3405	+54 57 15.327	149.77	3.25	8.5	124	V
TXS0418+532	04 22 44.4004	+53 24 26.240	151.32	2.61	10.1	143	V
TXS0424+551	04 28 46.3	+55 18 11	150.57	4.56	...	...	
TXS0428+445	04 31 48.1	+44 42 19	158.62	-2.36	...	...	
TXS0429+415	04 32 36.5044	+41 38 28.433	160.97	-4.34	25.0	347	V
TXS0435+487	04 38 59.1	+48 48 46	156.42	1.32	...	...	
TXS0436+426	04 40 07.8720	+42 44 40.251	161.08	-2.57	7.0	102	V
TXS0445+449	04 48 58.2	+45 02 01	160.39	0.13	...	...	
TXS0446+422	04 49 33.6	+42 17 46	162.56	-1.54	...	...	

TXS0447+408	04 50 43.5	+40 56 13	163.74	-2.25	13.8	152	
TXS0446+518	04 50 53.0	+51 56 34	155.27	4.79	...	...	
TXS0447+482	04 51 44.1	+48 19 48	158.16	2.60	...	...	
TXS0456+428	05 00 27.5	+42 53 28	163.36	0.39	6.2	69	
TXS0458+476	05 02 25.9	+47 46 05	159.71	3.65	...	...	
TXS0500+443	05 03 50.0	+44 24 38	162.53	1.80	7.1	79	
TXS0500+339	05 03 56.7859	+34 03 28.138	170.77	-4.47	6.1	72	V
TXS0501+380	05 04 42.3	+38 05 17	167.65	-1.91	...	...	
TXS0503+466	05 07 23.6580	+46 45 42.349	161.03	3.72	16.0	178	V
TXS0509+406	05 12 52.5	+40 41 43	166.50	0.92	28.7	431	
TXS0510+403	05 14 03.0	+40 25 23	166.85	0.94	...	...	
TXS0513+455	05 17 28.8994	+45 37 04.871	162.98	4.46	7.0	87	V
TXS0514+330	05 18 05.1438	+33 06 13.369	173.28	-2.65	10.4	164	V
TXS0514+374	05 18 10.1	+37 33 38	169.65	-0.07	...	...	
TXS0517+454	05 20 47.5	+45 28 35	163.43	4.86	...	...	
TXS0523+327	05 26 43.4	+32 50 09	174.53	-1.31	...	...	
TXS0526+373	05 30 12.7	+37 23 32	171.13	1.81	6.7	91	
TXS0532+391	05 35 55.1	+39 10 58	170.24	3.72	...	...	
TXS0534+342	05 37 45.1	+34 18 07	174.56	1.41	...	...	
TXS0537+356	05 40 52.9	+35 42 16	173.71	2.70	...	...	
TXS0539+290	05 42 11.9	+29 01 46	179.53	-0.59	...	...	
TXS0544+273	05 47 34.1490	+27 21 56.845	181.57	-0.45	11.8	183	IVM
TXS0545+276	05 49 06.8	+27 37 11	181.52	-0.02	...	...	
TXS0547+234	05 50 47.3	+23 26 48	185.30	-1.84	11.4	148	
TXS0549+192	05 52 25.8	+19 13 40	189.13	-3.66	6.5	84	
TXS0550+312	05 53 21.6	+31 17 51	178.83	2.65	...	...	
TXS0550+195	05 53 42.1	+19 36 30	188.95	-3.21	...	...	
TXS0556+238	05 59 32.0331	+23 53 53.926	185.92	0.12	22.5	336	IM
TXS0558+193	06 01 54.4	+19 23 16	190.11	-1.64	...	...	
TXS0600+177	06 03 09.1302	+17 42 16.810	191.72	-2.21	14.2	165	IM
TXS0600+219	06 03 51.5	+21 59 37	188.07	0.04	6.0	75	
TXS0600+299	06 03 55.8520	+29 57 05.339	181.14	3.95	...	...	V
TXS0601+245	06 04 55.5	+24 29 55	186.01	1.48	26.0	437	M
TXS0610+171	06 13 36.4	+17 08 25	193.43	-0.31	5.9	68	
TXS0610+260	06 13 49.1	+26 04 37	185.59	4.00	10.4	164	M
TXS0611+131	06 13 57.6934	+13 06 45.401	197.01	-2.16	21.6	256	IV
TXS0616+136	06 18 57.5	+13 36 32	197.15	-0.85	...	...	
TXS0616+051	06 19 00.2	+05 06 30	204.66	-4.84	...	...	
TXS0617+210	06 20 19.5286	+21 02 29.501	190.74	2.94	...	...	V
TXS0618+145	06 21 41.1	+14 32 11	196.64	0.17	...	...	
TXS0622+147	06 25 46.0	+14 40 19	196.98	1.10	5.0	59	
TXS0624+139	06 27 35.8	+13 56 50	197.83	1.16	...	...	
TXS0625+034	06 27 38.2	+03 24 59	207.17	-3.72	...	...	
TXS0626+077	06 29 06.7	+07 43 32	203.51	-1.40	...	...	
TXS0627+176	06 30 07.2587	+17 38 12.930	194.84	3.40	9.7	158	V
TXS0628+203	06 31 01.0614	+20 20 59.206	192.52	4.84	14.5	221	V
TXS0628+191	06 31 31.7	+19 08 33	193.65	4.39	...	...	
TXS0629+104	06 32 15.3	+10 22 02	201.53	0.51	5.1	62	
TXS0629+160	06 32 43.1349	+15 59 57.606	196.58	3.20	14.0	208	VM
TXS0630+082	06 33 13.0	+08 13 20	203.54	-0.27	...	...	

TXS0633+045	06 36 05.7	+04 32 41	207.14	-1.33	...	...	
TXS0634+013	06 36 56.5	+01 18 20	210.11	-2.63	...	...	
TXS0637+028	06 40 12.9	+02 50 57	209.12	-1.19	...	...	
TXS0638+098	06 41 45.1	+09 46 48	203.13	2.32	...	...	
TXS0639-032	06 41 51.0	-03 20 48	214.82	-3.66	16.0	362	
TXS0640+090	06 43 26.3	+08 57 38	204.05	2.31	12.5	176	
TXS0641-010	06 43 48.1	-01 08 21	213.08	-2.22	...	...	
TXS0641+127	06 43 59.8	+12 38 18	200.83	4.10	...	...	
TXS0642+055	06 45 16.7	+05 31 33	207.31	1.15	...	...	
TXS0645-023	06 48 29.0	-02 22 07	214.70	-1.74	...	...	
TXS0647-092	06 49 24.7	-09 18 37	221.01	-4.68	...	...	
TXS0647-018	06 50 25.7	-01 52 22	214.48	-1.08	...	...	
TXS0648-083	06 50 59.3	-08 23 52	220.37	-3.92	...	...	
TXS0650-063	06 53 00.7	-06 25 32	218.83	-2.58	7.1	308	
TXS0650-003	06 53 17.1	-00 23 02	213.48	0.24	...	...	
TXS0651+001	06 53 50.5	+00 05 08	213.13	0.57	...	...	
TXS0653-033	06 56 11.2	-03 23 06	216.49	-0.49	17.6	576	
TXS0656-062	06 59 03.2	-06 21 09	219.45	-1.21	...	...	
TXS0700-007	07 03 19.1	-00 51 01	215.04	2.25	28.3	390	
TXS0703-133	07 06 00.6	-13 24 32	226.52	-2.91	—	—	
TXS0704-003	07 07 29.9	-00 26 07	215.15	3.37	...	...	
TXS0705-079	07 07 49.6	-07 59 38	221.91	-0.03	...	...	
TXS0705-142	07 08 03.4	-14 21 15	227.59	-2.90	—	—	
TXS0706-042	07 08 38.9	-04 19 06	218.74	1.85	...	...	
TXS0706-153	07 09 12.2	-15 27 00	228.69	-3.16	—	—	
TXS0707-028	07 09 48.4	-02 56 22	217.65	2.74	...	...	
TXS0707-036	07 10 20.2	-03 43 27	218.40	2.50	11.0	133	
TXS0708+005	07 10 53.5	+00 26 49	214.75	4.53	...	...	
TXS0709+008	07 11 47.3	+00 48 19	214.54	4.89	...	...	
TXS0713-192	07 15 39.1	-19 20 05	232.85	-3.58	—	—	
TXS0713-024	07 15 46.9	-02 31 02	217.96	4.26	...	...	
TXS0714-165	07 16 59.6	-16 35 59	230.57	-2.03	...	...	
TXS0715-181	07 18 14.5	-18 12 59	232.14	-2.52	—	—	
TXS0718-152	07 20 44.3	-15 20 39	229.88	-0.64	...	...	
TXS0718-154	07 21 13.6	-15 30 38	230.09	-0.62	...	...	
TXS0718-119	07 21 21.9	-12 05 33	227.09	1.02	...	...	
TXS0719-187	07 22 09.5	-18 48 30	233.10	-1.97	—	—	
TXS0721-093	07 23 27.6	-09 25 45	224.98	2.73	...	...	
TXS0721-071	07 24 17.4	-07 15 18	223.15	3.93	12.5	218	
TXS0722-068	07 24 29.1	-06 58 08	222.92	4.11	...	...	
TXS0722-095	07 24 55.2	-09 39 57	225.36	2.93	...	...	
TXS0725-255	07 27 33.2	-25 36 31	239.70	-4.08	—	—	
TXS0727-221	07 29 26.1	-22 18 06	236.99	-2.13	—	—	
TXS0727-115	07 30 19.1124	-11 41 12.601	227.77	3.14	68.5	1270	IVM
TXS0728-262	07 30 42.3	-26 20 36	240.68	-3.80	—	—	
TXS0728-235	07 31 06.6	-23 41 49	238.40	-2.46	—	—	
TXS0729-223	07 31 31.9	-22 24 40	237.32	-1.76	—	—	
TXS0733-174	07 35 45.8125	-17 35 48.501	233.58	1.44	14.0	284	I
TXS0733-224	07 35 57.1	-22 32 59	237.93	-0.93	—	—	
TXS0738-137	07 40 20.5	-13 51 52	230.86	4.23	...	...	

TXS0739-266	07 41 55.4	-26 47 30	242.30	-1.83	—	—	
TXS0740-171	07 42 25.4	-17 15 11	234.06	3.00	...	...	
TXS0741-249	07 43 21.9	-25 03 09	240.95	-0.69	—	—	
TXS0741-183	07 43 32.2	-18 25 57	235.22	2.64	...	...	
TXS0744-158	07 46 18.5	-15 55 36	233.37	4.46	5.7	112	
TXS0745-191	07 47 31.4	-19 17 39	236.44	3.03	—	—	
TXS0745-165	07 48 03.1	-16 39 50	234.22	4.46	13.7	276	
TXS0749-191	07 51 23.1	-19 17 17	236.90	3.82	—	—	
TXS0750-219	07 52 35.9	-22 02 40	239.42	2.66	—	—	
TXS1729-244	17 32 05.7	-24 26 52	2.20	4.95	...	...	
TXS1744-193	17 47 14.4	-19 20 59	8.40	4.65	...	...	
TXS1748-253	17 51 51.2630	-25 24 00.060	3.74	0.63	...	...	I
TXS1749-224	17 52 33.2	-22 30 12	6.32	1.97	...	...	
TXS1750-187	17 53 09.0	-18 43 35	9.65	3.77	...	...	
TXS1752-225	17 55 26.0	-22 32 09	6.63	1.38	...	...	
TXS1754-226	17 57 27.7	-22 38 59	6.77	0.92	...	...	
TXS1755-162	17 58 41.5	-16 16 52	12.44	3.84	...	...	
TXS1755-179	17 58 43.3	-17 57 51	10.98	3.00	...	...	
TXS1759-224	18 02 13.1	-22 27 51	7.47	0.06	...	...	
TXS1800-218	18 03 05.0	-21 49 31	8.13	0.20	...	...	
TXS1800-278	18 03 16.7	-27 48 09	2.94	-2.78	...	...	
TXS1800-175	18 03 38.1	-17 32 25	11.92	2.19	...	...	
TXS1802-252	18 05 23.5	-25 12 38	5.44	-1.92	...	...	
TXS1806-200	18 09 00.8	-20 04 51	10.33	-0.16	...	...	
TXS1808-194	18 11 35.3	-19 26 04	11.18	-0.37	...	...	
TXS1811-179	18 14 15.1	-17 55 51	12.81	-0.21	...	...	
TXS1811-167	18 14 35.4	-16 45 32	13.87	0.28	...	...	
TXS1815-111	18 18 16.4	-11 08 09	19.25	2.17	...	...	
TXS1816-150	18 18 58.8	-15 00 28	15.92	0.19	...	...	
TXS1817-044	18 20 13.7	-04 25 42	25.41	4.89	...	...	
TXS1817-098	18 20 38.1	-09 47 17	20.71	2.29	...	...	
TXS1819-245	18 22 21.1	-24 30 03	7.90	-4.97	...	...	
TXS1819-096	18 22 28.8	-09 38 57	21.05	1.96	...	...	
TXS1822-173	18 25 36.6	-17 18 49	14.63	-2.30	7.2	130	
TXS1822-076	18 25 37.8	-07 37 28	23.20	2.21	6.6	131	
TXS1825-041	18 27 45.0411	-04 05 44.568	26.58	3.38	...	...	V
TXS1825-214	18 28 19.5	-21 23 37	11.30	-4.76	...	...	
TXS1825-055	18 28 39.8	-05 30 50	25.42	2.53	...	...	
TXS1829-106	18 32 20.8	-10 35 12	21.35	-0.63	29.0	564	
TXS1830-106	18 33 33.6	-10 34 06	21.50	-0.89	...	...	
TXS1831-073	18 34 10.3	-07 17 52	24.47	0.49	...	...	
TXS1835-055	18 38 16.4	-05 29 46	26.54	0.41	...	...	
TXS1836+040	18 38 48.8289	+04 04 24.637	35.13	4.66	11.4	191	V
TXS1836-125	18 39 30.4	-12 30 55	20.44	-3.07	...	...	
TXS1840-079	18 42 48.6	-07 56 06	24.89	-1.71	...	...	
TXS1840-036	18 43 16.9	-03 35 38	28.80	0.17	...	...	
TXS1841-043	18 44 22.4	-04 17 43	28.30	-0.39	...	...	
TXS1843-001	18 46 03.9	-00 03 38	32.27	1.17	5.6	76	
TXS1843-120	18 46 06.3	-11 58 09	21.66	-4.26	...	...	
TXS1843-030	18 46 27.2	-02 59 11	29.71	-0.25	...	...	

TXS1844-025	18 47 00.5	-02 27 52	30.23	-0.14	...	...	
TXS1844-001	18 47 04.5	-00 04 48	32.36	0.93	...	...	
TXS1845+018	18 47 44.0	+01 54 33	34.21	1.69	...	...	
TXS1847-092	18 50 29.7	-09 08 54	24.67	-3.95	...	...	
TXS1857+129	18 59 23.3	+12 58 55	45.40	4.15	...	...	
TXS1901+155	19 04 14.3609	+15 36 38.448	48.28	4.29	7.8	109	V
TXS1902+159	19 04 46.2	+16 03 15	48.74	4.38	...	...	
TXS1903+015	19 06 13.0	+01 39 13	36.09	-2.53	...	...	
TXS1904+013	19 07 11.9969	+01 27 08.974	36.02	-2.84	7.8	117	V
TXS1906+165	19 09 01.0	+16 39 45	49.75	3.75	...	...	
TXS1909+048	19 11 49.5	+04 58 57	39.69	-2.24	...	...	
TXS1910+052	19 12 54.2	+05 18 01	40.10	-2.34	13.4	170	
TXS1911+165	19 14 14.4	+16 36 39	50.28	2.62	7.7	96	
TXS1915+062	19 17 48.6	+06 21 22	41.60	-2.93	...	...	
TXS1916+062	19 19 17.3	+06 19 42	41.75	-3.27	6.5	81	
TXS1919+086	19 22 18.6	+08 41 57	44.20	-2.82	...	...	
TXS1920+154	19 22 34.6995	+15 30 10.024	50.23	0.33	17.2	219	V
TXS1921+174	19 23 33.7	+17 29 37	52.10	1.06	...	...	
TXS1922+204	19 24 36.5	+20 35 22	54.95	2.30	...	...	
TXS1922+155	19 24 39.4562	+15 40 43.931	50.63	-0.03	21.9	307	V
TXS1923+151	19 25 24.5	+15 14 17	50.32	-0.40	...	...	
TXS1923+210	19 25 59.6054	+21 06 26.162	55.56	2.26	40.3	624	IV
TXS1926+273	19 28 31.1	+27 26 58	61.43	4.76	...	...	
TXS1926+087	19 28 40.8554	+08 48 48.412	45.04	-4.15	7.4	89	I
TXS1927+256	19 29 44.9170	+25 43 16.223	60.03	3.70	5.6	68	V
TXS1928+154	19 30 52.8	+15 32 35	51.22	-1.41	25.0	323	
TXS1929+226	19 31 24.9167	+22 43 31.258	57.58	1.93	9.1	120	I
TXS1930+258	19 32 49.9	+25 59 05	60.60	3.21	...	...	
TXS1930+131	19 33 02.5	+13 13 40	49.44	-2.98	...	...	
TXS1931+149	19 33 21.8	+15 04 46	51.10	-2.16	5.4	77	
TXS1932+174	19 34 50.2	+17 32 15	53.43	-1.28	...	...	
TXS1937+214	19 39 35.6	+21 36 14	57.52	-0.27	...	...	
TXS1938+273	19 40 39.4	+27 30 37	62.78	2.43	...	...	
TXS1943+228	19 46 06.2519	+23 00 04.411	59.48	-0.88	5.7	71	I
TXS1944+250	19 46 47.2	+25 12 42	61.47	0.09	...	...	
TXS1945+267	19 47 26.3	+26 53 47	63.00	0.82	...	...	
TXS1945+241	19 48 01.4	+24 14 49	60.78	-0.63	...	...	
TXS1950+253	19 52 48.1	+25 26 51	62.37	-0.96	10.7	174	
TXS1954+282	19 56 46.5	+28 20 39	65.30	-0.22	10.1	152	
TXS1958+257	20 01 05.4	+25 51 46	63.69	-2.34	...	...	
TXS1959+241	20 01 54.0	+24 16 20	62.44	-3.33	...	...	
TXS2002+335	20 04 23.3	+33 39 06	70.67	1.19	...	...	
TXS2005+403	20 07 44.9449	+40 29 48.604	76.82	4.30	63.5	946	I
TXS2005+372	20 07 45.2	+37 22 01	74.18	2.61	7.8	105	
TXS2008+332	20 10 49.7	+33 22 13	71.16	-0.09	11.4	210	
TXS2013+340	20 15 28.8318	+34 10 39.406	72.37	-0.45	24.0	331	V
TXS2014+358	20 16 45.7	+36 00 33	74.04	0.36	6.8	94	
TXS2015+336	20 17 13.1	+33 45 46	72.23	-0.98	...	...	
TXS2018+295	20 20 06.5	+29 42 14	69.21	-3.77	9.2	141	
TXS2018+282	20 20 45.8719	+28 26 59.205	68.25	-4.59	...	...	V

TXS2021+317	20 23 19.0177	+31 53 02.307	71.40	-3.10	42.3	596	IV
TXS2023+335	20 25 10.8416	+33 43 00.218	73.13	-2.37	103.1	1496	IV
TXS2023+372	20 25 23.5	+37 23 14	76.15	-0.28	...	...	
TXS2024+296	20 26 59.3	+29 50 53	70.18	-4.91	...	...	
TXS2025+360	20 27 22.2	+36 12 14	75.42	-1.29	...	...	
TXS2027+464	20 29 18.9366	+46 36 02.269	84.08	4.48	...	...	V
TXS2048+361	20 50 02.2848	+36 19 52.500	78.29	-4.85	15.8	267	V
TXS2056+445	20 58 28.6	+44 46 17	85.80	-0.65	...	...	
TXS2117+494	21 18 52.4	+49 36 58	91.71	0.08	...	...	
TXS2118+443	21 20 31.7734	+44 34 34.281	88.32	-3.66	9.3	139	V
TXS2121+547	21 23 05.3161	+55 00 27.329	95.98	3.44	7.8	104	V
TXS2122+519	21 24 34.8	+52 07 15	94.11	1.22	...	...	
TXS2125+552	21 27 32.5	+55 28 33	96.76	3.33	...	...	
TXS2126+489	21 27 57.6	+49 10 31	92.45	-1.27	...	...	
TXS2130+556	21 32 09.5	+55 52 41	97.51	3.17	...	...	
TXS2135+508	21 37 00.9	+51 01 34	94.77	-0.90	13.6	199	
TXS2144+568	21 46 25.9398	+57 03 24.687	99.77	2.75	...	...	V
TXS2154+482	21 56 37.8	+48 30 28	95.58	-4.86	...	...	
TXS2156+596	21 58 29.5	+59 51 19	102.76	3.94	...	...	
TXS2159+505	22 01 43.5394	+50 48 56.393	97.65	-3.53	16.3	260	V
TXS2222+600	22 24 36.9	+60 16 16	105.67	2.42	10.9	142	
TXS2229+539	22 31 18.8	+54 09 36	103.26	-3.27	...	...	
TXS2238+610	22 40 20.0	+61 17 09	107.84	2.32	...	...	
TXS2244+635	22 46 13.8	+63 49 55	109.65	4.24	...	...	
TXS2247+596	22 49 28.7	+59 54 57	108.20	0.58	...	...	
TXS2250+644	22 52 05.5	+64 40 12	110.60	4.70	...	...	
TXS2252+576	22 54 53.8	+57 56 39	107.95	-1.50	...	...	
TXS2255+570	22 57 19.8	+57 20 33	107.99	-2.18	6.5	80	
TXS2259+568	23 01 26.6287	+57 06 25.508	108.39	-2.63	14.6	179	V
TXS2300+577	23 03 04.8	+58 03 23	108.98	-1.85	...	...	
TXS2303+599	23 05 10.3	+60 14 39	110.11	0.05	...	...	
TXS2307+627	23 09 21.1	+63 01 03	111.65	2.40	...	...	
TXS2336+598	23 39 21.2	+60 10 13	114.08	-1.46	9.6	153	
TXS2348+643	23 50 54.8	+64 40 20	116.51	2.56	...	...	

Column 1: Texas source name; Column 2 & 3: Source position in J2000; Column 4 & 5: Source position in Galactic coordinates; Column 6: Signal-to-noise ratio with Nobeyama-Kashima baseline; Column 7: correlated flux density at 22 GHz for Nobeyama-Kashima baseline. '—' in column 6 & 7 indicates that the source was not observed.; Column 8: 'I' denotes the source listed in ICRF catalog (Ma et al.1998), 'V' denotes the source listed in VLBA calibrator source (Peck & Beasley 1998), and 'M' denotes the source listed in 2 GHz VLBI survey (Morabito et al. 1986).

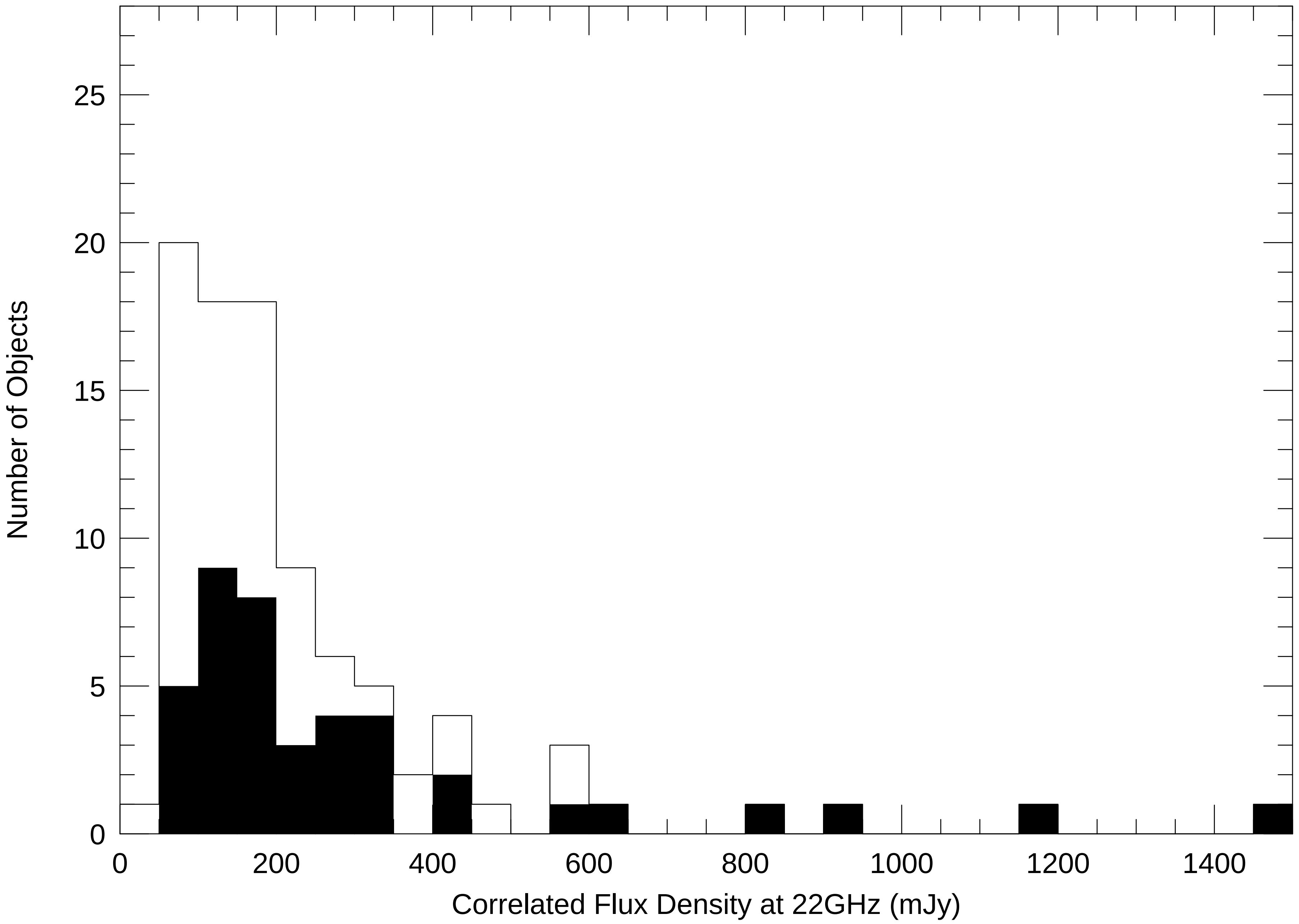
0
5
10
15
20
25
Number of Objects
0
200
400
600
800
1000
1200
1400
Correlated Flux Density at 22GHz (mJy)

arXiv:astro-ph/0004220v1 17 Apr 2000

Table 2. Positions for 21 VLBI sources measured with J-Net.

source	RA(J2000)	DEC(J2000)	ΔRA	ΔDEC	error
TXS0012+610	00 14 48.70	+61 17 42.8	0.00	-2.15	0.6
TXS0056+579	00 59 52.33	+58 12 24.1	1.05	0.10	1.2
TXS0106+612	01 09 46.34	+61 33 30.3	-2.15	-0.68	1.7
TXS0137+635	01 40 43.10	+63 46 07.0	0.00	0.03	0.2
TXS0203+625	02 07 02.74	+62 46 13.2	-0.25	0.22	0.5
TXS0205+643	02 09 35.97	+64 37 26.0	-0.55	-0.05	0.3
TXS0248+560	02 51 54.65	+56 16 19.5	-1.55	-0.50	0.6
TXS0354+559	03 58 30.37	+56 06 43.0	2.93	-1.00	0.4
TXS0509+406	05 12 52.53	+40 41 43.1	-0.45	0.08	0.4
TXS0547+234	05 50 47.33	+23 26 48.1	0.16	0.14	0.2
TXS0601+245*	06 04 55.03	+24 29 55.9	-6.89	0.94	0.2
TXS0640+090	06 43 26.44	+08 57 38.3	1.06	0.26	0.2
TXS0721-071	07 24 17.34	-07 15 17.3	-2.04	0.72	1.7
TXS1928+154	19 30 52.82	+15 32 35.0	-0.54	0.02	1.3
TXS1950+253	19 52 48.34	+25 26 55.9	2.45	4.93	0.3
TXS1954+282	19 56 46.05	+28 20 59.3	-6.09	20.30	0.3
TXS2005+372	20 07 45.44	+37 22 04.4	1.87	3.36	0.2
TXS2008+332	20 10 49.71	+33 22 15.2	-0.46	2.25	0.3
TXS2135+508	21 37 01.01	+51 01 36.4	0.47	2.41	0.2
TXS2255+570	22 57 22.06	+57 20 30.6	18.35	-2.43	0.5
TXS2336+598	23 39 21.26	+60 10 12.8	0.23	-0.21	0.3

Column 1: Texas source name; column 2 & 3: measured source position in J2000; column 4 & 5: position difference between positions measured in the present study and listed in Texas survey (Douglas et al.1996); column 6: position error in arcsec.

*: this source is listed in Morabito et al.(1986).